Eur Biophys J (2003) 32: 710–723
DOI 10.1007/s00249-003-0336-5

ARTICLE

K. Gast · A. J. Modler · H. Damaschun · R. Kröber
G. Lutsch · D. Zirwer · R. Golbik · G. Damaschun

Effect of environmental conditions on aggregation and fibril formation of barstar

Received: 4 October 2002 / Accepted: 18 June 2003 / Published online: 26 July 2003

Abstract The dependence on environmental conditions of the assembly of barstar into amyloid fibrils was investigated starting from the nonnative, partially folded state at low pH (A-state). The kinetics of this process was monitored by CD spectroscopy and static and dynamic light scattering. The morphology of the fibrils was visualized by electron microscopy, while the existence of the typical cross-β structure substantiated by solution X-ray scattering. At room temperature, barstar in the A-state is unable to form amyloid fibrils, instead amorphous aggregation is observed at high ionic strength. Further destabilization of the structure is required to transform the polypeptide chain into an ensemble of conformations capable of forming amyloid fibrils. At moderate ionic strength (75 mM NaCl), the onset and the rate of fibril formation can be sensitively tuned by increasing the temperature. Two types of fibrils can be detected differing in their morphology, length distribution and characteristic far UV CD spectrum. The formation of the different types depends on the particular environmental conditions. The sequence of conversion: A-state $\rightarrow$ fibril type I $\rightarrow$ fibril type II appears to be irreversible. The transition into fibrils is most effective when the protein chain fulfills particular requirements concerning secondary structure, structural flexibility and tendency to cluster.

K. Gast (✉) · A. J. Modler · H. Damaschun · R. Kröber
G. Lutsch · D. Zirwer · G. Damaschun
Max-Delbrück-Centrum für Molekulare Medizin,
Robert-Rössle-Str. 10, 13125 Berlin, Germany
E-mail: gast@mdc-berlin.de
Fax: +49-30-94062548

A. J. Modler
Institut für Biologie c/o Max-Delbrück-Centrum
für Molekulare Medizin,
Humboldt-Universität zu Berlin,
Robert-Rössle-Strasse 10, 13125 Berlin, Germany

R. Golbik
Abteilung Enzymologie, Institut für Biochemie,
Martin-Luther-Universität Halle-Wittenberg,
Kurt-Mothes-Str. 30, 06120 Halle, Germany

Keywords Barstar · Amyloid fibril · A-state · Aggregation · Protein folding · Secondary structure

Abbreviations *CD*: circular dichroism · *DLS*: dynamic light scattering · *EM*: electron microscopy · *SLS*: static light scattering · *SAXS*: small-angle X-ray scattering · *SOXS*: solution X-ray scattering

Introduction

Barstar is a protein, the folding mechanisms of which have been analyzed in great detail (Fersht 1998; Nölting 1999). In this work we report on misfolding of barstar. Amyloid fibrils and possibly prefibrillar oligomers play a crucial role in the development of diseases called amyloidoses (Rochet and Lansbury 2000; Pepys 2001) including Alzheimer's disease, Parkinson's disease and Prion diseases. Furthermore, there is growing evidence that many proteins of rather different amino acid composition, which are not related to any of these diseases, are able to form amyloid-like fibrils under special environmental conditions, for example the SH3 domain of phosphatidylinositol 3′-kinase (Guijarro et al. 1998), acylphosphatase (Chiti et al. 1999), phosphoglycerate kinase (PGK) from yeast (Damaschun et al. 1999, 2000) and apomyoglobin (Fändrich et al. 2001). Interestingly, even such sequences, which are not expected to be amyloidogenic according to their native structures, exhibit amyloid formation under specific conditions (Fezoui et al. 2000; Fändrich et al. 2001). Thus, the ability to form amyloid appears to be a generic property of polypeptide chains (MacPhee and Dobson 2000). Despite this clear evidence of fibril formation for an increasing number of sequences the process itself, particularly the early steps and the conformations that favor fibril formation, are still poorly understood in general. The structural properties of the so-called amyloid precursors favoring amyloid formation were identified on the level of individual amino acid residues only in the special cases of transthyretin

(Liu et al. 2000) and β_2-microglobulin (McParland et al. 2002). It is generally accepted that the starting point is the transition of the polypeptide chain into a partially folded intermediate state (Rochet and Lansbury 2000; Khurana et al. 2001). The characterization of this particular conformation and the intermolecular interactions of the polypeptide chain in this intermediate state are key issues for understanding amyloid fibril formation. It is still an open question, whether the amyloidogenic intermediates are more native-like having properties like a molten globule (Kuwajima 1989; Ptitsyn 1995), or have a more expanded conformation comprising several preformed secondary structural elements. We want to address this question by studying amyloid formation by barstar.

Barstar is the 89-residue polypeptide inhibitor of the ribonuclease barnase from *Bacillus amyloliquefaciens* (Hartley 1989). The three-dimensional structure of wild-type barstar was solved by NMR (Lubienski et al. 1994) and the structure of the C40A/C82A variant in complex with barnase by X-ray crystallography (Guillet et al. 1993; Buckle et al. 1994). Barstar is of α/β structure consisting of three strands of parallel β-sheet and four helices. The peptide bond to Pro-48 is in the *cis* conformation in the native state. Thus, *cis*/*trans* peptidyl-prolyl isomerization influences the folding kinetics. It is an excellent model protein for studying unfolding and refolding, association of a protein complex (Schreiber and Fersht 1996; Frisch et al. 2001) and catalysis of peptidyl-prolyl *cis*/*trans* isomerization (Golbik et al. 1999). Barstar shows the phenomenon of cold denaturation at easily attainable temperatures (Agashe and Udgaonkar 1995; Wong et al. 1996; Nölting et al. 1997). Refolding from the cold-denatured state can be triggered by ultra-fast temperature jump (T-jump) techniques (Ballew et al. 1996) allowing studies of the earliest folding events. In combination with Φ-value analysis (Fersht 1995), folding of barstar was resolved at the level of individual amino acids on the microsecond to second time scale (Nölting et al. 1995; Nölting 1997). Multiple pathways and multiple intermediates were observed both for folding (Shastry and Udgaonkar 1995) and unfolding (Zaidi et al. 1997).

At low pH, barstar undergoes a structural transition to an alternatively folded, nonnative conformation, the A-state (Fink et al. 1994). The A-state of barstar resembles the molten globule possessing the peculiarity of existing as a soluble oligomer with an apparent molecular mass of about 150,000 D (Khurana and Udgaonkar 1994; Khurana et al. 1995; Juneja et al. 2002). For comparison, the monomer mass of the pseudo wild-type variant C40A/C82A/P27A (Nölting et al. 1995) used in our studies is 10,252 D. Recent NMR investigations (Juneja et al. 2002) have identified and characterized flexible regions in the polypeptide chains forming the molten globule-like aggregate at low pH. Accordingly, the A-form appears to be a symmetrical aggregate of 16 monomers with a rigid core, but with the 20 N-terminal residues of each of the monomeric subunits in highly dynamic random chain conformation, which shows transient local ordering of structure.

Many proteins form fibrillar structures at low pH and in several cases small soluble aggregates were identified at early stages of this process. Accordingly, the multimeric A-form of barstar could be the starting point for fibrillization of this protein. Our results demonstrate that the molten globule-like aggregates of barstar at low pH do not form fibrillar structures at any ionic strength at room temperature. In particular, an increase of the NaCl concentration in order to diminish repulsive intermolecular interactions leads to the formation of amorphous, fractal aggregates. Further destabilization of the structure is required to transform the polypeptide chain into an ensemble of conformations capable of forming amyloid fibrils. Since barstar exhibits a high rate of amyloid formation under appropriate conditions, the onset of fibril formation could be clearly detected by gradually changing the environmental conditions, particularly by changing temperature and ionic strength. The growth process and the conversion of secondary structure were monitored by dynamic light scattering (DLS) and circular dichroism (CD) spectroscopy, respectively. The morphology of the fibrils at late stages was determined by electron microscopy (EM). The existence of cross-β structure typical of amyloid fibrils was substantiated by characteristic peaks in the solution X-ray scattering (SOXS) curves. Depending on the environmental conditions, two structural conversion processes leading to two different types of fibrils could be observed.

Materials and methods

Materials

The pseudo wild-type of barstar (C40A/C82A/P27A variant) was expressed and purified as described previously (Golbik et al. 1999). As a final purification step gelfiltration on Superdex 75 (Amersham Biosciences AB, Uppsala, Sweden) with 50 mM Tris-HCl buffer, pH 8.0, 0.1 M NaCl was performed. The molecular mass was controlled by electrospray mass spectrometry. Protein concentrations were determined from absorbance at 280 nm using a molar extinction coefficient of 22,690 l $mol^{-1}cm^{-1}$. Different conformational states of barstar were obtained by dialyzing the protein into the individual solvents specified in the figure legends. For investigations of the A-state at different NaCl concentrations, solutions of barstar in 10 mM HCl were mixed with concentrated NaCl solutions containing 10 mM HCl.

Methods

Light scattering measurements

Dynamic and static light scattering were measured simultaneously with one and the same instrument at a scattering angle of 90°. The present laboratory-built apparatus, which consisted mainly of an argon laser Lexel 3500 (Lexel Laser Inc., Fremont, Calif., USA) operating at 514.5 nm wavelength and 0.5 W output power, a thermostat-controlled cell holder and a photon detection system, equipped with a high quantum yield avalanche photodiode, was described in detail in Gast et al. (1997). The solvents and protein solutions were filtered through 100 nm pore-size Anotop filters (Whatman, Maidstone UK) directly into small flow-through cells with pathlength of 0.8 and 1.5 mm (Hellma,

Müllheim, Germany). Molar masses were calculated from the relative scattering intensities using toluene as a reference sample. The homodyne time-autocorrelation functions of the scattered light intensity $g(\tau)$ were calculated by a 90-channel multibit multiple-τ correlator. The translational diffusion coefficients D were obtained from $g(\tau)$ using either the program CONTIN (Provencher 1982) or by applying the method of cumulants (Koppel 1972). The diffusion coefficients were converted into Stokes radii via the Stokes–Einstein equation $R_S = k_B T/(6\pi\eta_0 D)$, where k_B is Boltzmann's constant, T is the temperature in K, and η_0 is the solvent viscosity. Solvent viscosities and densities were measured using an Ubbelohde type viscometer Viscoboy 2 (Lauda, Lauda-Königshofen, Germany) and a digital density meter DMA 58 (Anton Paar, Graz, Austria), respectively. Refractive indices of the solvent mixtures were measured with an Abbe type refractometer.

CD measurements

CD measurements were carried out on a J-720 (JASCO, Japan) CD spectrometer, which was calibrated with (+)-camphorsulfonic acid at 290.5 and 192.5 nm (Johnson 1990). For measurements in the near UV region, 5- and 10-mm pathlength cells and protein concentrations between 0.5 and 1 mg/ml were used. CD measurements in the far UV region were made with 0.1-mm and 1-mm pathlength cells and at protein concentrations of about 1 and 0.15 mg/ml, respectively. Mean residue molar ellipticities $[\theta]$ were calculated using the mean residue weight of 113.9. Kinetic CD spectra were recorded using the interval-scan modus of the JASCO software. This scheme allows to store a number of succeeding CD spectra separately. The measuring time for one spectrum can be optimized by choosing a particular wavelength range, spectral resolution and integration time. A time resolution of about 30 s could be obtained with a sufficiently high signal-to-noise ratio in this way. If necessary, an improvement of the quality of the CD spectrum can be obtained by repeating the kinetic experiment.

In order to get an idea of the changes in secondary structure, analysis of the CD spectra was carried out using three methods for secondary structure estimation from CD, SELCON3, CDSSTR and CONTIN/LL included in the software package CDPro (Sreerama and Woody 2000). Several reference protein sets are available for data evaluation. We have used that containing 48 reference proteins including also five unfolded proteins throughout. Only for the analysis of the native state spectrum the reference set containing 43 folded proteins was used for comparison. The results of these estimations are tabulated in a condensed form. For this purpose, we have averaged the results of the three methods, reduced the secondary structural classes to α helix, β strand, turn and unordered, and omitted errors in these estimations in the table. Briefly, relative errors vary strongly (approximately between $\pm 5\%$ and $\pm 50\%$) depending on the type and on the proportion of a particular structure.

Solution and small-angle X-ray scattering (SOXS and SAXS)

SOXS and SAXS were measured in the step-scan mode on a transmission X-ray diffractometer equipped with five-slit apertures and using CuK_α radiation. Details have been described recently (Damaschun et al. 2000). The scattering curves were measured at 260 points in the interval from $s_{min} = 0.21$ nm^{-1} to $s_{max} = 31$ nm^{-1}, where $s = (4\pi/\lambda)\sin\theta$. λ is the wavelength of the X-ray radiation and 2θ is the scattering angle. The scattering curves were measured in 10 mM HCl and 75 mM NaCl, at room temperature and at a protein concentration of 21 mg/ml. Prior to the measurement, the sample was incubated for 45 min at 70 °C. Desmearing of the scattering curves, calculation of the cross-section scattering curves and calculation of the radius of gyration of the cross-section were performed by the program SAXS (Damaschun et al. 2000).

Electron microscopy

Before preparation for electron microscopy, barstar solutions were diluted to a protein concentration of about 30 μg/ml with the corresponding solvent. Barstar was visualized by negative staining with 1% uranyl formate using a double-carbon film technique.Four-hundred mesh copper grids covered with a carbon-coated triafol microgrid were used as support. Micrographs were taken with an EM910 electron microscope (LEO, Oberkochen, Germany) at 80 kV and a magnification of 63,000.

Results

Structural properties of the A-state at 20 °C—influence of ionic strength

The A-state of barstar was obtained by dialyzing the protein from native conditions (50 mM Tris-HCl, pH 8, 100 mM KCl) into 10 mM HCl. The structural changes were monitored by measuring the CD spectra in the near and far UV regions and by static (SLS) and dynamic light scattering (DLS). In order to get an idea of the degree of unfolding at acid pH, we have also measured the same conformational parameters for well characterized highly unfolded states, namely the unfolded state at 6 M urea and the cold-denatured state. Figure 1a shows the far UV CD spectra of barstar in the native and cold-denatured states and in the A-state in both the absence and presence of salt. The spectrum of cold-denatured barstar is typical of a polypeptide chain lacking essentially ordered secondary structure. A similar spectrum in a somewhat limited spectral range $\lambda > 212$ nm was obtained in 6 M urea (data not shown). By contrast, a spectrum with native-like features was obtained for barstar in 10 mM HCl (A-state) indicating that an essential amount of secondary structure still exists under these environmental conditions. Increasing ionic strength (addition of NaCl in the present case) favors the formation of secondary structure changing the spectrum towards the native one. The corresponding change in secondary structure is complete at NaCl concentrations above 75 mM (inset Fig. 1a). Despite the existing secondary structure, the A-state is lacking rigid side chain packing typical of stable tertiary structure both in the absence and presence of salt. This is indicated by the strongly diminished near UV CD spectra which are similar to that in the cold-denatured state (Fig. 1b). These results are in general agreement with data previously reported in the literature (Khurana and Udgaonkar 1994; Nölting et al. 1997).

Molar masses obtained from SLS and Stokes radii R_S, translational diffusion coefficients D and diffusive virial coefficients k_D obtained from DLS are summarized in Table 1. Barstar ($M_{calculated} = 10{,}252$ g/mol) is monomeric and compact in the native state at pH 8. On the transition to the unfolded state in 6 M urea or to the cold-denatured state, the Stokes radius increases by 65% or 45%, respectively. While the highly unfolded protein is monomeric according to the measured light scattering intensity, the increased Stokes radius in

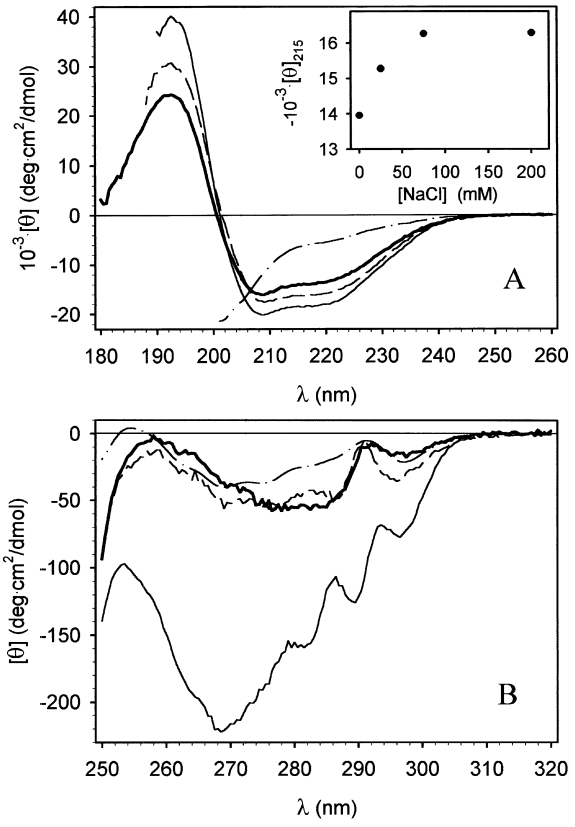

Fig. 1 a Far UV and **b** near UV CD spectra of barstar in different conformational states: *thin line* native state at 20 °C in 50 mM Tris-HCl, pH 8, 0.1 M KCl; *dash–dot line* cold-denatured state at 1 °C in 50 mM Tris-HCl, pH 8, 0.1 M KCl, 2.2 M urea; *thick line* A-state in 10 mM HCL at 20 °C; *dashed line* A-state in 10 mM HCl, 75 mM NaCl at 20 °C; the inset of panel A shows the dependence on NaCl concentration of the specific ellipticity at 215 nm in the A-state at 20 °C

the A-state is mostly a consequence of oligomerization as can be seen from the increased molar mass. Except for the native state, the masses in Table 1 represent weight average masses (see below). The existence of oligomers prevents the estimation of the Stokes radius of individual protein molecules under these conditions. The average size and the temporal stability of the molten globule-like oligomer at pH 2 and 20 °C are influenced by the ionic strength. In the absence of salt, the oligomers consist of about five monomers on average. The size of the oligomers increases with addition of salt (NaCl in the present case) according to our light scattering data (Table 1). The size increase levels off above 75 mM NaCl when an average size corresponding to about 15 monomers is reached. While the size of the oligomers does not change remarkably over the period of several days at NaCl concentrations below 75 mM, a growth process was observed at higher salt concentrations. This growth process was monitored by measuring both the apparent average mass by SLS (Fig. 2) and the apparent average Stokes radius by DLS at 200 mM NaCl using a sample with 1 mg/ml protein concentration. Apparent quantities are measured when extrapolation to zero protein concentration is not performed. The size distribution calculated by CONTIN consisted essentially of one relatively narrow peak. Accordingly, the average radius of this peak and the average radius obtained from the cumulant analysis agreed very well. Fitting the relative increase $R_{S,app}/R_{S,mon}$ versus M_{app}/M_{mon} plotted in a logarithmic scale to a straight line (inset of Fig. 2) is a useful procedure for determining the dimensionality of the growth process. The value of the slope of 0.49 corresponds to a dimensionality of 2.04, being typical of a growth process leading to the formation of amorphous aggregates as shown by EM (Fig. 7A). The far UV CD spectrum of the sample was controlled for more than 100 h. Remarkably it remained unchanged in pattern and amplitude within the experimental error of about ± 2%.

Temperature-induced structural changes of the A-form in the absence of salt

The changes in secondary structure on heating barstar in 10 mM HCl from 20 °C up to 80 °C were monitored by far-UV CD. Instead of a cooperative transition a more gradual change of the spectrum towards that of a polypeptide chain with little ordered secondary structure was observed (Fig. 3a). At temperatures above 40 °C gradual melting of the secondary structure was

Table 1 Stokes radii R_S, translational diffusion coefficients D, diffusive virial coefficients k_D, and molar masses M of barstar under the influence of different environmental conditions. Except for the native state, the values are averages over an ensemble of configurations

Condition	R_S (nm)	$D\times10^7$ (cm^2/s)	k_D (mL/g)	$M\times10^{-3}$ (g/mol)
Native conditions,[a] 20°C	1.72 ± 0.04	12.5 ± 0.3	5 ± 3	9.96 ± 0.45
Unfolded at 6 M urea, 20°C	2.83 ± 0.07	7.57 ± 0.19	50 ± 20	n.d.[d]
Cold denatured at 1°C and 2.2 M urea	2.50 ± 0.06	8.58 ± 0.21	-3 ± 3	n.d.
A-state,[b] no salt, 20°C	4.96 ± 0.24	4.32 ± 0.21	210 ± 50	51 ± 10
A-state, 75 mM NaCl, 20°C	5.88 ± 0.29	3.64 ± 0.18	12 ± 3	150 ± 30
Fibrillar state[c]	34 ± 1	0.63 ± 0.03	55 ± 8	3,800 ± 700

[a]50 mM Tris-HCl, pH 8, 100 mM KCl (this solvent was also used in the case of the unfolded and cold-denatured states).
[b]10 mM HCl, pH 2.
[c]10 mM HCl, pH 2, 75 mM NaCl, 20°C after incubating the sample for 15 min at 70°C.
[d]Not determined.

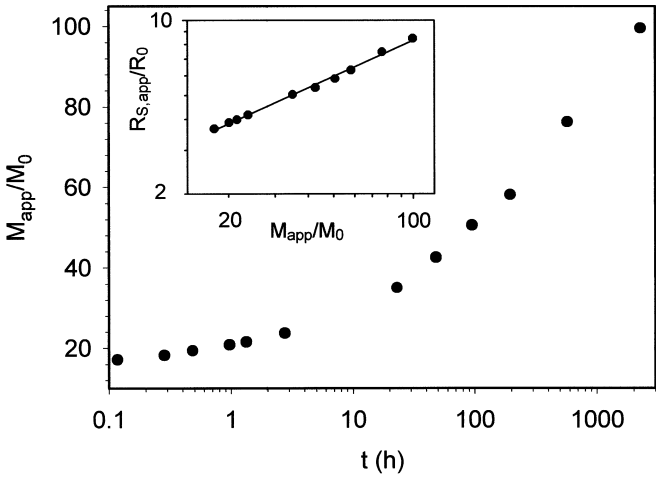

Fig. 2 Time dependence of the relative apparent mass M_{app}/M_0 for barstar in the A-state in 10 mM HCl, pH 2, 200 mM NaCl at 20 °C. *Inset* Relative apparent Stokes radius $R_{S,app}/R_0$ vs. relative apparent mass under the same conditions. M_0 and R_0 are the molecular mass and the Stokes radius of the monomeric protein under native conditions, respectively

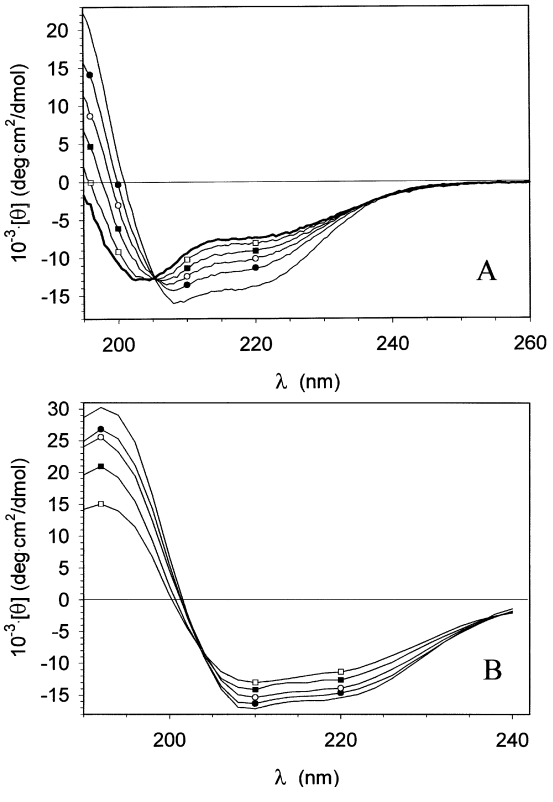

Fig. 3a, b Temperature dependence of the far UV CD spectrum of barstar in 10 mM HCL (A-state). **a** In the absence of salt: *thin line* 20 °C; *solid circles* 40 °C; *open circles* 50 °C; *solid squares* 60 °C; *open squares* 70 °C; *thick line* 80 °C. **b** In the presence of 75 mM NaCl immediately after approaching the particular temperatures: *thin line* 20 °C; *solid circles* 40 °C; *open circles* 50 °C; *solid squares* 60 °C; *open squares* 70 °C

accompanied by disaggregation of the oligomers reflected by a decrease in light scattering intensity and in Stokes radius (data not shown). A new steady state in aggregate size was reached within 20–30 min after a temperature change. The average mass calculated for the quite narrow size distribution was comparable with that of a dimer at 70 °C. The sample was kept at each measuring temperature at least for 1 h and at the highest temperature for 3 h to detect any slower time-dependent structural changes. No further changes in secondary structure and aggregation or disaggregation processes were observed even at protein concentrations above 1 mg/ml. The heat-induced structural changes were essentially reversible. The spectrum after cooling down to 20 °C was in between the spectra at 20 °C and 40 °C during heating.

Temperature-induced structural changes of the A-form and amyloid formation in the presence of salt

If not otherwise stated, these experiments were performed in 10 mM HCl and 75 mM NaCl. Under these conditions, salt-induced changes in secondary structure of the A-form are completed and aggregation is still negligible at room temperature. Most of the CD spectra were recorded in a special kinetic modus (see Materials and methods), which allowed us to record a sufficiently large spectral range (192–240 nm in Fig. 3b) in less than 1 min. This capability turned out to be very important for measuring CD spectra at elevated temperatures because two kinds of temperature-induced spectral changes were observed. The first one was caused by fast partial unfolding proceeding within the dead time of the experiment. The second one was caused by a subsequent reorganization of the secondary structure, which occurred at higher temperatures within a time range of minutes. The time evolution of the second process could be resolved using the kinetic CD approach. The time constant of the T-jump from 20 °C to each measuring temperature was about 20 s. Spectra immediately after T-jumps from 20 °C to the specified temperatures are shown in Fig. 3b. They are characteristic of the partially unfolded state of barstar at these temperatures. A comparison with the corresponding spectra in Fig. 3a clearly shows the structure stabilizing effect of 75 mM NaCl. The spectrum at 70 °C in the presence of salt indicates a considerable amount of secondary structure even at elevated temperatures (Table 2).

The same spectrum is again shown in Fig. 4a in order to compare it with the altered, but stable final spectrum measured 40 min after the T-jump. Such time-dependent changes of the CD spectrum occurred above 50 °C indicating the formation of ordered, but misfolded secondary structure (Table 2) at elevated temperatures. The absorption of the CD samples did not noticeably change during this conversion process. Thus, a distortion of the final CD spectrum due to scattering artefacts can be ruled out. The temporal changes of the CD signal at

Table 2 Secondary structure content calculated from far UV CD spectra using the software package CDPro (Sreerama and Woody 2000)

State	Condition	Spectrum in	Helix (%)	β-strand (%)	Turn (%)	Unordered (%)
Native state 48/43 ref. proteins[a]	50 mM Tris, pH 8, 0.1 M KCl	Fig. 1a	59	6	12	23
A-state 20°C	10 mM HCl, pH 2, 75 mM NaCl	Fig. 1a	47	13	16	24
Conversion I						
A-state 70°C	10 mM HCl, pH 2, 75 mM NaCl	Figs. 3b/4a	33	18	21	29
Fibrils type I 70°C	10 mM HCl, pH 2, 75 mM NaCl	Fig. 4A	40	17	19	25
Fibrils type I 20°C	10 mM HCl, pH 2, 75 mM NaCl	Fig. 5	45	17	17	22
Conversion II						
Fibrils type I 70°C	10 mM HCl, pH 2	Fig. 8	34	18	20	29
Intermediate 70°C	10 mM HCl, pH 2	Fig. 8	29	18	20	34
Fibrils type II 70°C	10 mM HCl, pH 2	Fig. 8	35	20	19	26

[a]The analysis for the native state was done using the reference protein sets including either 43 folded proteins or 43 folded and five unfolded proteins (the results do not differ after rounding to integers). The reference set with 43 folded and five unfolded proteins was used for the other states. Concerning the errors in the calculated values, see Materials and methods

215 nm measured at 55 °C, 65 °C and 70 °C are shown in Fig. 4b. The horizontal bar in Fig. 4b indicates the CD at 20 °C before heating. Different CD amplitudes were observed immediately after heating at the various temperatures caused by different degrees of unfolding. The time course of the unfolding reaction could not be resolved by our experimental approach. The time constants of the subsequent changes in the CD signal decreased considerably with increasing temperature. We have characterized the rate of the conversion process in terms of reciprocal half times $t_{1/2}$ of the total changes. The rates are shown in an Arrhenius plot in Fig. 4c. An activation energy of 19.2 ± 2.0 kcal/mol was obtained from the slope. Nearly identical CD spectra were measured for samples incubated at temperatures between 55 °C and 70 °C for sufficiently long times.

The CD spectrum measured at 20 °C after heat-induced conversion during the kinetic CD experiment at 70 °C is shown in Fig. 5. Different samples incubated under identical environmental conditions showed practically identical CD spectra indicating that a defined secondary structure was formed in a reproducible manner during conversion. According to an analysis of the spectra before and after heat-induced conversion (Table 2) the major change in secondary structure is an increase in β structure. The reliability of the secondary structure estimations will be discussed later.

The increase in β structure could be an indication of the formation of intermolecular β structure such as cross-β structure as found in amyloid fibrils. An unequivocal decision cannot be made using CD data alone. However, the formation of cross-β structure is well reflected by characteristic peaks in solution X-ray scattering curves. The SOXS curve of barstar incubated for 45 min at 70 °C (data not shown) revealed a broad maximum and sharp peaks at scattering vectors $s = 6$ nm^{-1} and $s = 13.3$ nm^{-1}, respectively. According to the Bragg equation $d = 2\pi s^{-1}$, the values of s correspond to distances $d = 1.05$ nm and 0.47 nm, which are characteristics of cross-β structure. The X-ray scattering curve of barstar was nearly identical to that of phosphoglycerate kinase (PGK) from yeast in the fibrillar state (Damaschun et al. 2000). This finding and the observed conversion on the level of secondary structure pointed to the formation of amyloid fibrils. This was confirmed by the results of SLS and DLS measurements and electron microscopy.

The conversion of the small protein aggregates consisting of about 15 monomers into larger structures was reflected by the time dependence of the relative apparent Stokes radius, $R_{S,app}/R_{S,mon}$, after a T-jump from 20 °C to 70 °C. This is shown for protein concentrations of 0.9 mg/ml and 4.3 mg/ml in Fig. 6a. A rough estimate of the half times of the fast size transition yielded 1.8 ± 0.2 min and 1.7 ± 0.2 min for $c = 0.9$ mg/ml and 4.3 mg/ml, respectively. The conversion process could be stopped at any time by lowering the temperature below ≈50 °C. The differences in $R_{S,app}$ at 0.9 mg/ml and 4.3 mg/ml right after the first, steep transition (Fig. 6a) are the result of intermolecular interactions (virial effects). This was checked by measuring the concentration dependence of R_S and D after conversion using a sample of high initial concentration (7 mg/ml), which was incubated for 15 min at 70 °C. The results of the measurements in terms of the diffusive virial coefficient k_D are given in Table 1. Thus, both the rate of conversion characterizing the first size transition and the resulting average size are practically independent of protein concentration. However, the protein concentration influences the growth process at later times. The average size remained constant at concentrations below 1 mg/ml. At higher concentrations, a second concentration-dependent growth process became evident (see the data for $c = 4.3$ mg/ml in Fig. 6a). The rate of this process was very low. More information about the growth characteristics can be obtained from the dimensionality of the entire size transformation process by plotting $R_{S,app}/R_{mon}$ versus M_{app}/M_{mon} in a logarithmic scale. This has been done for the data obtained at 4.3 mg/ml in Fig. 6b. An abrupt increase in the slope corresponding to a decrease in dimensionality is connected with the transition from the first (fast) to the second (very slow) size transition.

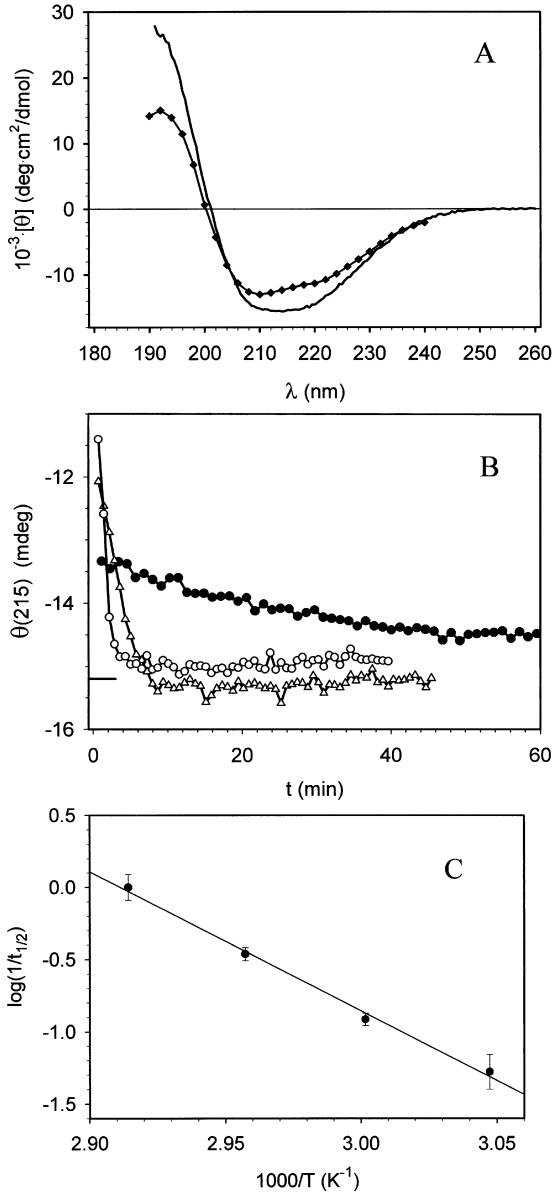

Fig. 4 **a** CD spectra of barstar $c = 1.08$ mg/ml during incubation at 70 °C in 10 mM HCl, 75 mM NaCl. *Diamonds* amyloidogenic intermediate state immediately after a T-jump from 20 °C to 70 °C; *thin line* after 40 min, when conversion is completed. **b** Time dependence of the ellipticities at 215 nm of barstar ($c = 1.08$ mg/ml, $d = 0.102$ mm) in 10 mM HCl, 75 mM NaCl after T-jumps from 20 °C to the specified temperatures. *Solid circles* 55 °C; *open triangles* 65 °C; *open circles* 70 °C. **c** Arrhenius plot of the corresponding reciprocal half times measured at 55 °C, 60 °C, 65 °C and 70 °C. The slope yields an activation energy $E_A = 19.2 \pm 2.0$ kcal/mol

Morphology of the fibrils

The initial and final slopes in Fig. 6b yield dimensionalities of 1.58 and 1.13 for the early and late stages of the structural transition, respectively. A dimensionality close to one corresponds to a strictly linear growth process. The somewhat larger observed values hint at the formation of elongated, but not completely straight

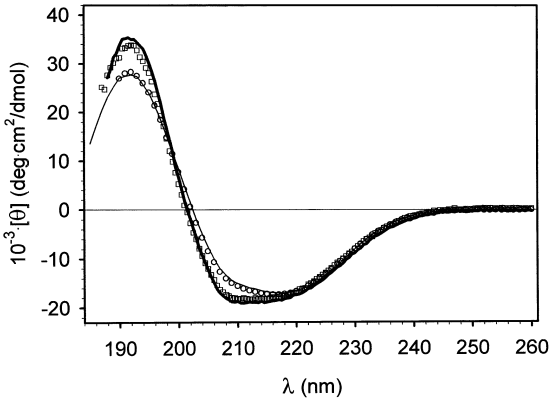

Fig. 5 Two types of CD spectra of barstar measured at 20 °C after temperature-induced structural conversion under the following conditions. Type I: *open square* $c = 1.01$ mg/ml, 55 min at 70 °C in 10 mM HCl, 75 mM NaCl; *thick line* 1.09 mg/ml, 75 min at 70 °C in 10 mM HCl, 75 mM NaCl (diluted SOXS sample). Type II: *open circle* $c = 1.15$ mg/ml, 105 min at 80 °C in 10 mM HCl, 75 mM NaCl; *thin line* $c = 0.92$ mg/ml, 70 min at 70 °C in 10 mM HCl, no salt

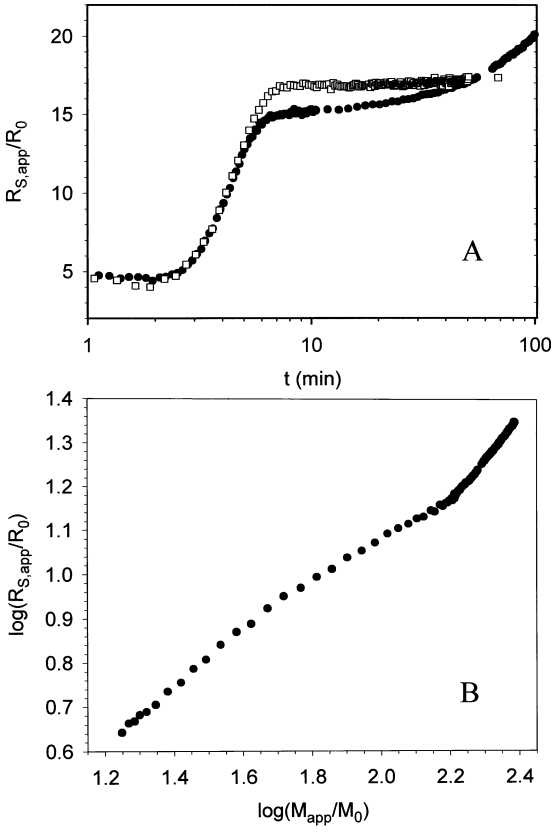

Fig. 6 **a** Time dependence of the relative apparent Stokes radius $R_{S,app}/R_0$ of barstar in 10 mM HCl, pH 2, 75 mM NaCl at 70 °C measured at concentrations of 0.9 mg/ml (*open squares*) and 4.3 mg/ml (*solid circles*). The experiment was started immediately after inserting the sample cell into the cell holder. The sample approached the specified temperature after about 2 min. **b** Plot of the relative apparent Stokes radius vs. relative apparent mass in logarithmic scale for the data obtained at 4.3 mg/ml

particles. For a closer inspection of their morphology we have performed EM investigations with diluted samples previously investigated by CD or DLS. Figure 7b shows the fibrillar structure of barstar aggregates in 10 mM HCl, 75 mM NaCl after 1 h of incubation at 70 °C at a concentration of 0.16 mg/ml. Under these conditions only the first size transition had occurred (cf. Fig. 6a). The fibrils show a twisted wormlike structure with a length of about 40–300 nm and a pitch of about 100 nm. Their width varies between about 6 nm and 13 nm. Additional information concerning the thickness of the fibrils is available from SAXS (Damaschun et al. 2000). From SAXS (data not shown) a radius of gyration of cross-section $R_C = 2.80 \pm 0.05$ nm was obtained. This is consistent with either a diameter of 7.93 nm for a circular cross-section or with main axes $a = 10.0$ nm and $b = 5.0$ nm for an elliptic cross-section. The latter result is in good agreement with the EM data. These structures will be termed fibrils of type I.

When concentrated solutions ($c = 7$ mg/ml) were incubated for about 3 h at 70 °C the formation of a second type of fibrillar structure could be observed. Short segments apparently consisting of three individual strands became visible (arrows and inset in Fig. 7c). This type of fibril is fully developed under conditions described below. It is characterized by a straight ribbon-like structure with a width of about 16 nm and a length of several micrometers (Fig. 7d). The fibrils are composed of three protofilaments in parallel arrangement instead of the twisted arrangement described above for fibrils of type I. Conversion from type I into type II was seen occasionally within the same fibril (arrow heads in Fig. 7c and d).

Fig. 7a–d Electron micrographs of negatively stained samples of barstar after different structural conversions. **a** Barstar 1.0 mg/ml stored for about 5 weeks in 10 mM HCl, pH 2, 200 mM NaCl at room temperature; **b** barstar 0.16 mg/ml in 10 mM HCl, pH 2, 75 mM NaCl incubated for about 1 h at 70 °C; **c** barstar 7 mg/ml in 10 mM HCl, pH 2, 75 mM NaCl incubated for 3 h at 70 °C; the inset shows conversion of a fibril from the first to the second type; **d** fibrils of the second type obtained by incubating fibrils of the first type ($c = 1.03$ mg/ml) for about 2 h at 70 °C in 10 mM HCl, pH 2. *Arrows* indicate fibrils of the second type. *Arrowheads* point to morphological transitions from fibrils of the first type to those of the second type. All samples were diluted prior to negative staining (see Materials and methods). *Bar* = 0.1 μm

Stability of type I fibrils and the transition into fibrils of type II

We have studied the stability of the fibrils of type I (cf. Fig. 7b) and the reversibility of the fibrillization process leading to their formation. Samples incubated at 70 °C in the presence of 75 mM NaCl exhibited small reversible temperature-dependent changes of the far UV CD spectrum, but did not show any temporal changes of this spectrum and of the average Stokes radius after cooling down to room temperature. Furthermore, no changes of these features were observed when the ionic strength was lowered by dialyzing the sample exhaustively against 10 mM HCl. Thus, the fibrils were stable under conditions, which do not favor their formation.

A further check of stability was performed by heating fibrils of type I in the absence of salt. Under this influence, the oligomers of the A-form had shown the tendency to dissociate. The CD spectrum of fibrils of type I in the absence of salt (data not shown) exhibited perceptible, but reversible changes at temperatures below 60 °C. Unexpectedly, on heating up to 70 °C, an

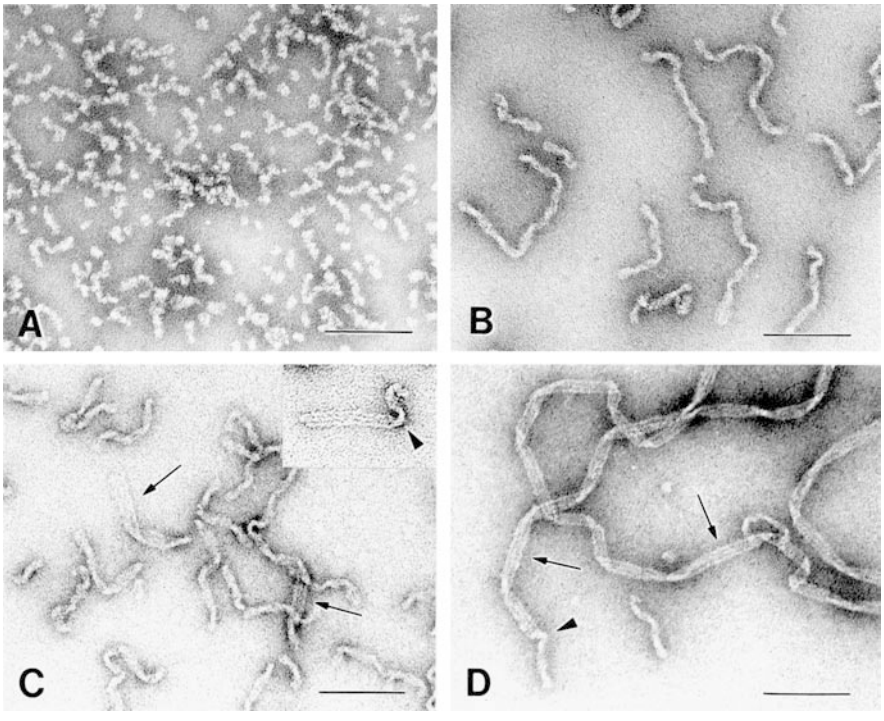

irreversible conversion of the CD spectrum was observed. Kinetic CD measurements (Fig. 8) revealed that this conversion process proceeds via an intermediate, which is maximally populated about 5 min after a T-jump from 20 °C to 70 °C. According to the pattern of the spectrum and secondary structure estimations using CDPro (Table 2), this state is more unfolded than the states right after the T-jump and at the end of the conversion process. Despite characteristic differences in the CD spectra before and after the second conversion process, analysis of the CD spectra (Table 2) indicated only a weak tendency towards formation of ordered secondary structure, particularly an increase in the percentage of β strands. The second conversion process was accompanied by a more than two-fold increase in the average Stokes (data not shown). The morphology of the fibrils formed in this way, termed type II fibrils, is shown in Fig. 7d. Such a fast and complete conversion was never observed at 70 °C in the presence of 75 mM NaCl. However, incubation of fibrils of type I at 80 °C in the presence of 75 mM NaCl initiated a similar fast transition leading to a CD spectrum indistinguishable from that after conversion at 70 °C in the absence of NaCl (Fig. 5). Accordingly the CD spectra are an easily identifiable signature of the various types of fibrils.

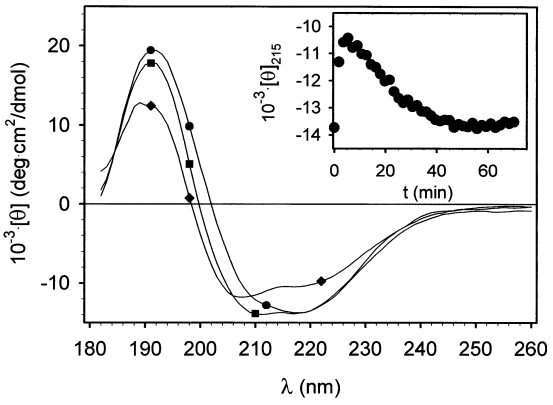

Fig. 8 Conversion of fibrils type I into fibrils type II at 70 °C, 10 mM HCl and in the absence of salt monitored by far UV CD. The protein concentration was 0.92 mg/ml. The conversion was initiated by rapidly changing the temperature from room temperature to 70 °C (dead time about 25 s). Three out of a total of 64 spectra are shown: *solid squares* immediately after heating; *diamonds* 5.8 min after heating (see *inset*); *solid circles* 70 min after heating (last spectrum). The inset shows the temporal changes of the specific ellipticity at 215 nm taken from the spectra

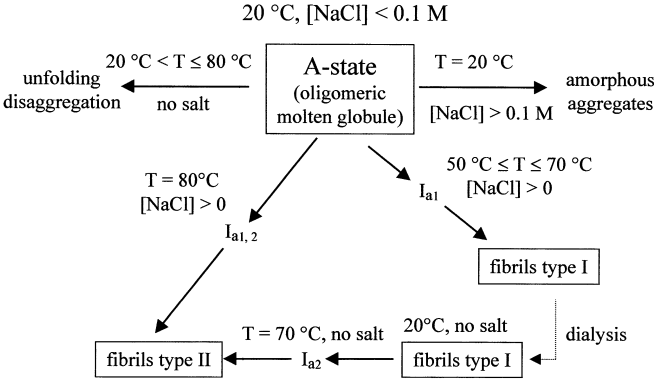

Fig. 9 Conversion scheme of barstar at pH 2 and different environmental conditions. Conversion into fibrils in the presence of salt ([NaCl] > 0) was found at salt concentrations as low as 25 mM. In all cases, the transitions proceeded via intermediate states. The properties of the identified intermediates I_{a1} and I_{a2} are described in the text. The transfer of type I fibrils to modified environmental conditions is indicate by the dotted line

Discussion

The A-state of barstar is not capable of forming amyloid at room temperature

In the following, we want to discuss the conditions influencing amyloid formation by barstar. A simple scheme showing the different structures and the transitions between them observed so far is given in Fig. 9. The horizontal arrows indicate two special cases, heating in the absence of salt and increase in the ionic strength at room temperature, which do not favor fibril formation because only one of two important preconditions for fibril formation is fulfilled. According to our CD spectroscopic investigations, the A-state of barstar at pH 2 and 20 °C comprises a content of regular secondary structure, which is almost comparable with that of the native state (Table 2), but has no fixed tertiary structure. We have estimated the secondary structure content in different states from the measured CD spectra using the software package CDPro (Sreeerama and Woody 2000). The results in Table 2 are average values of the data obtained from the individual programs SELCON3, CDSSTR and CONTIN/LL included in this package. Use of the reference protein set containing 43 folded proteins and in addition five unfolded proteins appeared to be an appropriate procedure, because most of the spectra measured in this study are related to partially unfolded states. The results of secondary structure estimations from CD data must be considered with caution, particularly the calculated percentage of secondary structure classes other than α-helical structure. This becomes evident when the CD spectrum of barstar in the native state is analyzed. According to the NMR structure (Lubienski et al. 1994), barstar contains 51% helical and 21% β structure. While the percentage of helical structure is in fair agreement with the NMR data, the amount of β structure is clearly underestimated (Table 2). This conflict does not result from the use of the reference set containing unfolded proteins, because an analysis using only folded proteins yielded the same results. This raises the question of whether the amount of β structure is underestimated in the analysis of other spectra shown in Table 2. Since an adequate error discussion for all cases in Table 2 is not feasible within the scope of this paper, errors have not been specified. The results in Table 2 should rather indicate the tendency of secondary structural changes upon the transitions between different states.

Following the nomenclature of Fink et al. (1994), barstar behaves like a type II protein upon acid denaturation. The compactness of individual barstar molecules in the A-state remains unknown because barstar forms oligomeric aggregates under conditions, where this partially folded state exists. Concerning the size of the molten globule-like oligomers, our results are consistent with those previously obtained by sedimentation velocity measurements (Khurana et al. 1995). Our SLS and DLS data reveal that the size and overall compactness of these aggregates increase with increasing ionic strength until a particular aggregate size of about 15 protein molecules is reached at 75 mM NaCl. This process is accompanied by a small increase in the amount of regular secondary structure, but rigid side chain packing is still absent. Further increase in NaCl concentration has no influence on secondary structure, initial size, and compactness of the aggregates, but results in a temporal instability of the aggregate size. The aggregates grow according to a scaling law $R = a \cdot M^{0.49}$ or $M = a^{-1} \cdot R^{2.04}$ (inset of Fig. 2), where a is a constant. The exponent corresponding to the dimensionality of 2.04 is close to the fractal dimension of 2.1 observed for reaction-limited cluster aggregation (Schüler et al. (1999) and references cited therein). The growth process leads to amorphous aggregates as shown in Fig. 7a. It is important to note that in the case of this aggregation process there is no coupling with changes on the level of secondary structure. Conversion into amyloid could not be observed at any ionic strength at room temperature. Aggregates consisting of more than 100 protein molecules were detected after storing a sample for several weeks. There is growing evidence that in many cases the existence of precursor aggregates exceeding a critical size is necessary for fibril formation (Bitan et al. 2001; Xu et al. 2001). Because the observed size ($M \sim 10^6 \cdot D$) is far beyond such a critical size this condition is fulfilled in the present case. Thus, we conclude that the chain conformation and the degree of conformational fluctuations of barstar in the A-state at room temperature are not favorable to initiate a structural conversion into amyloid fibrils. These properties are characteristic of a special case, where fibril formation is not feasible. Further destabilization of the chain conformation is necessary to initiate fibril formation.

Temperature-induced amyloid formation—fibrils of type I

Our results have shown that barstar can exist in several different conformational states with different degrees of aggregation under the same environmental conditions at acid pH depending on the previously applied external conditions. Therefore, it is necessary to clarify that the term A-state will be used only for those protein molecules, which have not been converted into amyloid structure. Barstar in the A-state in 10 mM HCl and in the absence of salt shows the following features upon heating up to 80 °C. The temperature dependence of the far UV CD spectrum (Fig. 3a) reveals that ordered secondary structure in the A-state is diminished in a non-cooperative manner at elevated temperatures. Concurrently, the ability of the A-state to form small oligomeric aggregates decreases with increasing temperature. The latter finding is not an obvious result since hydrophobic interactions increase with increasing temperature. However, the observed disaggregation at higher temperatures could explain, why fibril formation is not observed at elevated temperatures in the absence of salt and preformed fibrillar structures. Under these conditions, strong repulsive electrostatic forces inhibit clustering of barstar molecules, which is essential for obtaining a critical size of aggregates. This is important to note, since considerable changes in secondary structure and in aggregate size (length and cross-section of fibrils) were observed under the same environmental conditions with pre-incubated samples consisting of fibrils of type I, viz., where the protein aggregates exceed a critical size (see below). Thus, heating barstar in the A-state in the absence of salt is the second special case that does not lead to fibril formation: individual protein molecules are expected to have sufficiently high conformational flexibility, but the conversion process is suppressed, because the ability of the protein molecules to cluster is too weak.

Both preconditions for fibril formation are fulfilled when barstar is heated in the presence of salt. Basically, the addition of salt has two main consequences. First, it stabilizes the existing secondary structure as can be seen by comparing the temperature dependence of the far UV CD spectra in the absence and presence of salt (Fig. 3a, b). Second, it strongly reduces repulsive intermolecular interactions. This is reflected by the decrease in the magnitude of the diffusive virial coefficient k_D (Table 1). Increase in temperature leads to partial unfolding of the protein, but even at 70 °C a considerable amount of secondary structure exists.

The corresponding transition leading to fibrillar structures is shown on the right-hand side of Fig. 9. The two consecutive arrows indicate the two-step character of the entire transition consisting of the unfolding reaction and the subsequent re-organization/aggregation process. The temperature-induced unfolding reaction was faster than the dead time of CD detection in experiments starting from the A-state. Disaggregation of existing small aggregates (about 15 monomers) was not detected at this stage. Increase in temperature shifts the ensemble of partly folded conformations towards an ensemble of more unfolded conformations. This new ensemble represents the amyloidogenic species and is termed $I_{a,1}$. The conformational properties of barstar in this state are characterized by the CD spectrum shown in Fig. 3b and Fig. 4a. The subsequent irreversible conversion towards a misfolded structure proceeded at NaCl concentrations as low as 25 mM. However, most of the experiments were done at 75 mM NaCl because of the higher conversion rate. At this salt concentration,

conversion is noticeable above 50 °C and the conversion rate is strongly dependent on temperature (Fig. 4b, c). In all cases, the conversion was coupled with the fast size transition (Fig. 6a), which led to the formation of flexible, worm-like fibrils with lengths between about 40 nm and 300 nm (Fig. 7b), termed fibrils of type I. The half time of the first size transition was found to be independent of protein concentration within the experimental error at least within the investigated concentration range above 0.2 mg/ml. Accordingly, the fast size transition and the accompanying secondary structure conversion process possess an apparent reaction order of one. Since aggregation is involved, which requires bimolecular reaction steps, the overall process must be governed by a preceding unimolecular reaction. This rate-limiting reaction represents an additional conformational transition of the A-state oligomers, which is required for their ability to aggregate during subsequent irreversible bimolecular reaction steps. This behavior resembles the scenarios devised by Lumry and Eyring (1954) in their seminal work on irreversible conformational changes of proteins. Recently (Roberts 2003), these scenarios found a quantitative representation in mathematical terms including a formal description of the bimolecular reaction steps.

The rate-limiting conformational transition leading to the misfolded conformation is connected with crossing of an energy barrier, for which we have calculated an activation energy $E_A = 19.2 \pm 2.0$ kcal/mol from the temperature dependence of the conversion rates of the CD signal (Fig. 4c). We can only speculate about details of the conversion process. It is noteworthy that the strong acceleration of the conversion process between 55 °C and 70 °C is connected with only minor secondary structure changes on average according to the changes of the far UV CD spectrum (Fig. 3b). We suppose that under the present solvent conditions and at temperatures above 50 °C the conformational fluctuations reach a critical state, which enables a sufficiently large ensemble of unspecifically aggregated protein molecules to undergo a rather cooperative transition into a critical oligomer with typical cross-β structure. This transition, which probably involves a substantial structural reorganization of the partially folded protein molecules, is characterized by an activation energy of about 20 kcal/mol. This process could be similar to some kind of domain swapping, which is observed during formation of oligomeric protein structures and was also proposed as a possible mechanism for amyloid formation (Janowski et al. 2001; Liu et al. 2001). On the other hand, a total reorganization of the structure of the polypeptide chains must be taken into consideration. The latter view is supported by recent studies of the core of β_2-microglobulin amyloid fibrils (Hoshino et al. 2002). The existence or formation of sufficiently large aggregates prior to this conversion process is obviously an important requirement during fibrillogenesis of barstar and also other proteins. This is supported by the fact that conversion proceeds only in the presence of salt, where initially formed oligomeric aggregates do not disaggregate on heating. Unraveling the full details of this conversion process is a central problem in studying amyloidosis.

The transitions in far UV CD and in R_S roughly coincide. At 70 °C, the half times of the initial fast process are 1 min and 1.7 min for the changes in CD and R_S, respectively. The high rate of conversion is very useful in exploring the conditions for the onset of fibril formation. However, this makes it very difficult to synchronize the CD and light scattering experiments adequately to compare changes in secondary structure and size in more detail. Up to now, we could not detect other critical aggregates smaller than the fibrillar structures. The first size conversion process stops rather abruptly and the resulting average size appears to be independent of protein concentration. Therefore, the termination is probably caused by depletion of the small oligomeric structures. Accordingly, the conversion process is kinetically irreversible. The strong decrease of the growth rate after the first transition (Fig. 6A), which shows that further length growth by end-to-end association is not efficient. While the size distribution was stable at low protein concentrations, a slow further increase in size could be detected above 1 mg/ml. This growth process is obviously coupled with a rarely occurring second transition of the internal structure of the fibrillar aggregates (see below). The fibrillar structures are characterized by a typical far UV CD spectrum. This was confirmed by comparing the CD spectra of individual samples of different protein concentrations incubated at 70 °C in the presence of 75 mM NaCl (Fig. 5).

The short fibrils of type I formed at elevated temperatures are stable at room temperature and against lowering the ionic strength. Dialysis against 10 mM HCl did not change the average size and the far UV CD spectrum. This clearly demonstrates the thermodynamic irreversibility of the conversion process under the tested external conditions. Nevertheless, the far UV CD spectrum exhibited perceptible, but reversible changes between 20 °C and 60 °C. This means that the structure of the fibrils of the first type is not rigid and is possibly susceptible to further temperature-induced structural transitions. This becomes indeed evident when the temperature is raised above 65 °C in the absence of salt.

Influence of environmental conditions on the type of fibril formation

Besides the fast conversion of barstar into short fibrils of type I at 70 °C and in the presence of 75 mM NaCl, a second structural conversion process was observed under particular conditions. The existence of the short fibrils was a requirement for all subsequent structural conversion processes under all conditions tested so far. Further structural conversion leading to much longer fibrils as shown in Fig. 7d could be observed under the following conditions: as a second slow process at 70 °C, 75 mM NaCl and high protein concentrations; as a second

process at 80 °C and 75 mM NaCl; during incubation of short fibrils of the first type at 70 °C in the absence of salt. The first condition is very unfavorable because of the low conversion rate and the rare appearance of the new type of fibrils. Thus, it is not shown in the general scheme (Fig. 9). The latter condition yielded the highest rate of conversion and was used to study this process in more detail. The fibrils formed during the second conversion are not only much longer, but have a different cross-section and morphology. Three individual protofilaments in parallel arrangement are clearly visible. According to light scattering and EM, these fibrils are formed without desintegration of the fibrils of type I. The inset of Fig. 7c shows that individual short fibrils are able to convert into the second type of fibrils. It is likely that three protofilaments already exist within the initial fibril, but the strands are strongly intertwined and can therefore not be visualized by EM.

Fibrils of different morphology depending on solution conditions have been reported also by other authors (Kad et al. 2001; Zurdo et al. 2001). An important property of type II fibrils is the much stronger ability for end-to-end association leading to the formation of very long fibrils (Fig. 7d). Information concerning the energetic barrier between fibrils of the first and the second type has not been obtained so far. Kinetic CD measurements (Fig. 8) revealed that the entire structural transition is again a two-stage process and proceeds via an intermediate $I_{a,2}$ with considerably less regular secondary structure compared to the initial and final states (Table 2). This means that a remarkable reorganization of the fibrils at the level of secondary structure is necessary to attain the second fibril type. The processes of partial unfolding and subsequent refolding into an altered misfolded structure proceeded with half times of about 1.5 min and 25 min, respectively. Obviously, these conformational transitions are coupled with partial untangling and reassembling of filaments of fibrils. This could explain why unfolding of secondary structure within fibrils of type I is considerably slower than unfolding starting from the A-state, where this step is fully buried within the dead time of the experiment. The fibrils of the second type are at least as stable as those of the first type. The reverse transition from fibrils of the second type to fibrils of the first type could not be observed. Both fibrillar structures correspond to discrete supramolecular states, which are characterized by a typical morphology and by a typical secondary structure according to the characteristic patterns of the CD spectra. This is demonstrated for fibrils of type II in Fig. 5 by the identical CD spectra of samples incubated either at 70 °C and in the absence of salt or at 80 °C in the presence of 75 mM NaCl.

The fibrils of type I observed in this study are very similar to protofibrillar structures observed during amyloidogenesis of many proteins. The fibrils of type II resemble more mature fibrils—however, they are lacking the high stiffness characteristic of this type of fibrils. According to discussions in the literature, it is not clear what types of protein aggregates are indeed the toxic species in conformational diseases. In addition to mature fibrils, protofibrillar or other prefibrillar structures are discussed as possible causes of some neurodegenerative diseases (Conway et al. 2000; Haass and Steiner 2001). For example, it has been shown that early stages of Alzheimer's disease are caused by small oligomers of the Aβ(1–42) peptide (Selkoe 2002). Thus, in addition to mature fibrils also other misfolded and aggregated structures and the mechanisms leading to their formation have to be studied in more detail.

Conclusions

We have shown that barstar can be converted into misfolded, fibrillar structure at low pH and elevated temperatures. The oligomeric molten-globule state itself is not capable of forming amyloid. The amyloidogenic species is rather a substantially destabilized, aggregation competent conformation that can be obtained by heating barstar in the presence of salt. The onset and the speed of fibrillogenesis of barstar can be sensitively and easily tuned by varying ionic strength and temperature. Accordingly, barstar is a useful model polypeptide to study the complicated interplay between specific intermolecular interactions and specific conformational states of the individual polypeptide chains, which essentially determines the transition of proteins into fibrillar structures. The results have underlined the important relation between structural polymorphism and environmental conditions.

While barstar undergoes a transition into fibrillar structure only under the relatively extreme conditions of low pH and elevated temperature, other proteins, particularly those involved in amyloidoses are prone to form fibrils under more physiological conditions. Interestingly, many disease-related sequences, e.g., the Aβ(1–42) peptide and α-synuclein, have an essentially unfolded conformation under physiological conditions. This is in accordance with our result on barstar that a more unfolded conformation than that of the molten globule-like A-state is essential for the ability to form fibrils.

Acknowledgements This work was supported by a grant from the Deutsche Forschungsgemeinschaft (Da 292/6–2) and by a grant from the Fonds der Chemischen Industrie to G.D.

References

Agashe VR, Udgaonkar JB (1995) Thermodynamics of denaturation of barstar: evidence for cold denaturation and evaluation of the interaction with guanidine hydrochloride. Biochemistry 34:3286–3299

Ballew RM, Sabelko J, Gruebele MRA (1996) Observation of distinct nanosecond and microsecond protein folding events. Nat Struct Biol 3:923–926

Bitan G, Lomakin A, Teplow DB (2001) Amyloid β-protein oligomerization. J Biol Chem 276:35176–35184

Buckle AM, Schreiber G, Fersht AR (1994) Protein–protein recognition: crystal structural analysis of a barnase–barstar complex at 2.0-A resolution. Biochemistry 33:8878–8889

Chiti F, Webster P, Taddei N, Clark A, Stefani M, Ramponi G, Dobson CM (1999) Designing conditions for in vitro formation of amyloid protofilaments and fibrils. Proc Natl Acad Sci USA 96:3590–3594

Conway KA, Harper JD, Lansbury PT (2000) Fibrils formed in vitro from α-synuclein and two mutant forms linked to Parkinson's disease are typical amyloid. Biochemistry 39:2552–2563

Damaschun G, Damaschun H, Gast K, Zirwer D (1999) Proteins can adopt totally different folded conformations. J Mol Biol 291:715–725

Damaschun G, Damaschun H, Fabian H, Gast K, Kröber R, Wieske M, Zirwer D (2000) Conversion of yeast phosphoglycerate kinase into amyloid-like structure. Proteins Struct Funct Gen 39:204–211

Fändrich M, Fletcher MA, Dobson CM (2001) Amyloid fibrils from muscle myoglobin—even an ordinary globular protein can assume a rogue guise if conditions are right. Nature 410:165–166

Fersht AR (1995) Characterizing transition states in protein folding—an essential step in the puzzle. Curr Opin Struct Biol 5:79–84

Fersht AR (1998) Structure and mechanism in protein folding. WH Freeman, New York

Fezoui Y, Hartley DM, Walsh DM, Selkoe DJ, Osterhout JJ, Teplow DB (2000) A de novo designed helix-turn-helix peptide forms nontoxic amyloid fibrils. Nat Struct Biol 7:1095–1099

Fink AL, Calciano LJ, Goto Y, Kurotsu T, Palleros DR (1994) Classification of acid denaturation of proteins: intermediates and unfolded states. Biochemistry 33:12504–12511

Frisch C, Fersht AR, Schreiber G (2001) Experimental assignment of the structure of the transition state for the association of barnase and barstar. J Mol Biol 308:69–77

Gast K, Nöppert A, Müller-Frohne M, Zirwer D, Damaschun G (1997) Stopped-flow dynamic light scattering as a method to monitor compaction during protein folding. Eur Biophys J 25:211–219

Golbik R, Fischer G, Fersht AR (1999) Folding of barstar C40A/C82A/P27A and catalysis of the peptidyl–prolyl *cis*/*trans* isomerization by human cytosolic cyclophilin (Cyp18). Protein Sci 8:1505–1514

Guijarro JI, Sunde M, Jones JA, Campbell ID, Dobson CM (1998) Amyloid fibril formation by an SH3 domain. Proc Natl Acad Sci USA 95:4224–4228

Guillet V, Lapthorn A, Hartley R, Mauguen Y (1993) Recognition between a bacterial ribonuclease, barnase, and its natural inhibitor, barstar. Structure 1:165–176

Haass C, Steiner H (2001) Protofibrils, the unifying toxic molecule of neurodegenerative disorders? Nature Neurosc 4:859–860

Hartley RW (1989) Barnase and barstar: two small proteins to fold and fit together. Trends Biochem Sci 14:450–454

Hoshino M, Katou H, Hagihara Y, Hasegawa K, Naiki, H, Goto Y (2002) Mapping the core of the β_2-microglobulin amyloid fibril by H/D exchange. Nat Struct Biol 9:332–336

Janowski R, Kozak M, Jankowska E, Grzonka Z, Grubb A, Abrahamson M, Jaskolski M (2001) Human cystatin C, an amyloidogenic protein, dimerizes through three-dimensional domain swapping. Nat Struct Biol 8:316–320

Johnson WC Jr (1990) Protein secondary structure and circular dichroism: a practical guide. Proteins 7:205–214

Juneja J, Bhavesh NS, Udgaonkar JB, Hosur RV (2002) NMR identification and characterization of the flexible regions in the 160 kDa molten globule-like aggregate of barstar at low pH. Biochemistry 41:9885–9899

Kad NM, Thomson NH, Smith DP, Smith DA, Radford SE (2001) beta(2)-microglobulin and its deamidated variant, N17D form amyloid fibrils with a range of morphologies in vitro. J Mol Biol 313:559–571

Khurana R, Udgaonkar JB (1994) Equilibrium unfolding studies of barstar: evidence for an alternative conformation which resembles a molten globule. Biochemistry 33:106–115

Khurana R, Hate AT, Nath U, Udgaonkar JB (1995) pH dependence of the stability of barstar to chemical and thermal denaturation. Protein Sci 4:1133–1144

Khurana R, Gillespie JR, Talapatra A, Minert LJ, Ionescu ZC, Millett I, Fink AL (2001) Partially folded intermediates as critical precursors of light chain amyloid fibrils and amorphous aggregates. Biochemistry 40:3525–3535

Koppel DE (1972) Analysis of macromolecular polydispersity in intensity correlation spectroscopy. The method of cumulants. J Chem Phys 57:4814–4820

Kuwajima K (1989) The molten globule state as a clue for understanding the folding and cooperativity of globular-protein structure. Proteins 6:87–103

Liu K, Cho HS, Lashuel HA, Kelly JW, Wemmer DE (2000) A glimpse of a possible amyloidogenic intermediate of transthyretin. Nat Struct Biol 7:754–757

Liu Y, Gotte G, Libonati M, Eisenberg D (2001) A domain-swapped RNase A dimer with implications for amyloid formation. Nat Struct Biol 8:211–214

Lubienski MJ, Bycroft M, Freund SM, Fersht AR (1994) Three-dimensional solution structure and ^{13}C assignments of barstar using nuclear magnetic resonance spectroscopy. Biochemistry 33:8866–8877

Lumry R, Eyring H (1954) Conformation changes of proteins. J Phys Chem 58:110–120

MacPhee CE, Dobson CM (2000) Formation of mixed fibrils demonstrates the generic nature and potential utility of amyloid nanostructures. J Am Chem Soc 122:12707–12713

McParland VJ, Kalverda AP, Homans SW, Radford SE (2002) Structural properties of an amyloid precursor of β_2-microglobulin. Nat Struct Biol 9:326–331

Nölting B (1997) The folding pathway of a protein at high resolution from microseconds to seconds. Proc Natl Acad Sci USA 94:826–830

Nölting B (1999) Protein folding kinetics (biophysical methods). Springer, Berlin Heidelberg New York

Nölting B, Golbik R, Fersht AR (1995) Submillisecond events in protein folding. Proc Natl Acad Sci USA 92:10668–10672

Nölting B, Golbik R, Soler-González AS, Fersht AR (1997) Circular dichroism of denatured barstar suggests residual structure. Biochemistry 36:9899–9905

Pepys MB (2001) Pathogenesis, diagnosis and treatment of systemic amyloidosis. Philos Trans R Soc Lond B Biol Sci 356:203–210

Provencher SW (1982) CONTIN: a general purpose constrained regularization program for inverting noisy linear algebraic and integral equations. Comput Phys Commun 27:229–242

Ptitsyn OB (1995) Molten globule and protein folding. Adv Protein Chem 47:83–229

Roberts CJ (2003) Kinetics of irreversible protein aggregation: analysis of extended Lumry–Eyring models and implications for predicting protein shelf life. J Phys Chem B 107:1194–1207

Rochet JC, Lansbury PT (2000) Amyloid fibrillogenesis: themes and variations. Curr Opin Struct Biol 10:60–68

Schreiber G, Fersht AR (1996) Rapid, electrostatically assisted association of proteins. Nat Struct Biol 3:427–431

Schüler J, Frank J, Saenger W, Georgalis Y (1999) Thermally induced aggregation of human transferrin receptor studied by light scattering techniques. Biophys J 77:1117–1125

Selkoe DJ (2002) Alzheimer's disease is a synaptic failure. Science 298:789–791

Shastry MCR, Udgaonkar JB (1995) The folding mechanism of barstar—evidence for multiple pathways and multiple intermediates. J Mol Biol 247:1013–1027

Sreerama N, Woody RW (2000) Estimation of protein secondary structure from circular dichroism spectra: Comparison of CONTIN, SELCON, and CDSSTR methods with an expanded reference set. Anal Biochem 287:252–260

Wong KB, Freund SMV, Fersht AR (1996) Cold denaturation of barstar: ^{1}H, ^{15}N and ^{13}C NMR assignment and characterisation of residual structure. J Mol Biol 259:805–818

Xu S, Bevis B, Arnsdorf M (2001) The assembly of amyloidogenic yeast sup35 as assessed by scanning (atomic) force microscopy: an analogy to linear colloidal aggregation? Biophys J 81:446–454

Zaidi FN, Nath U, Udgaonkar JB (1997) Multiple intermediates and transition states during protein unfolding. Nat Struct Biol 4:1016–1024

Zurdo J, Guijarro JI, Jimenez JL, Saibil HR, Dobson CM (2001) Dependence on solution conditions of aggregation and amyloid formation by an SH3 domain. J Mol Biol 311:325–340